ACS Photonics

Article

pubs.acs.org/journal/apchd5

Using n- and p-Type Bi_2Te_3 Topological Insulator Nanoparticles To Enable Controlled Femtosecond Mode-Locking of Fiber Lasers

Yung-Hsiang Lin,[†] Sheng-Fong Lin,[†] Yu-Chieh Chi,[†] Chung-Lun Wu,[†,‡] Chih-Hsien Cheng,[†] Wei-Hsuan Tseng,[†] Jr-Hau He,[†] Chih-I Wu,[†] Chao-Kuei Lee,[‡] and Gong-Ru Lin*[,†]

[†]Graduate Institute of Photonics and Optoelectronics, and Department of Electrical Engineering, National Taiwan University (NTU), 1, Roosevelt Road Section 4, Taipei 10617, Taiwan, R.O.C.

[‡]Department of Photonics, National Sun Yat-San University (NSYSU), Kaohsiung, 70 Lienhai Road, Kaohsiung 80424, Taiwan, R.O.C.

ABSTRACT: Mechanically triturated n- and p-type Bi_2Te_3 nanoparticles, the nanoscale topological insulators (TIs), are employed as nonlinear saturable absorbers to passively mode-lock the erbium-doped fiber lasers (EDFLs) for sub-400 fs pulse generations. A novel method is proposed to enable the control on the self-amplitude modulation (SAM) of TI by adjusting its dopant type. The dopant type of TI only shifts the Fermi level without changing its energy bandgap, that the n- and p-type Bi_2Te_3 nanoparticles have shown the broadband saturable absorption at 800 and 1570 nm. In addition, both the complicated pulse shortening procedure and the competition between hybrid mode-locking mechanisms in the Bi_2Te_3 nanoparticle mode-locked EDFL system have been elucidated. The p-type Bi_2Te_3 with its lower effective Fermi level results in more capacity for excited carriers than the n-type Bi_2Te_3, which shortens the pulse width by enlarging the SAM depth. However, the strong self-phase modulation occurs with reduced linear loss and highly nonsaturated absorption, which dominates the pulse shortening mechanism in the passively mode-locked EDFL to deliver comparable pulse widths of 400 and 385 fs with n- and p-type Bi_2Te_3 nanoparticles, respectively. The first- and second-order Kelly sidebands under soliton mode-locking regime are also observed at offset frequencies of 1.31 and 1.94 THz, respectively.

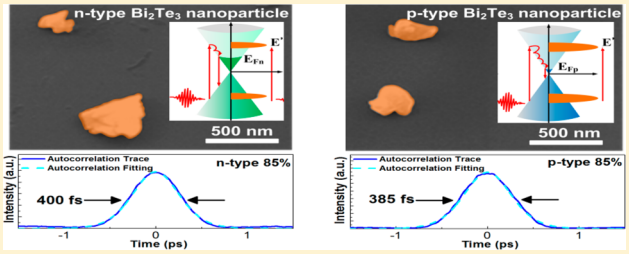

KEYWORDS: *Bi_2Te_3 nanoparticle, topological insulator, passive mode-locking, femtosecond soliton laser, pulse compression*

Ultrafast fiber lasers have found numerous applications in optical communications, micromachining,[1] biophotonic imaging,[2] and fundamental scientific research.[3] Passive mode-locking of fiber laser using saturable absorber is a typical method of generating ultrashort pulse. The development of a broadband, ultrafast saturable absorber that is conveniently fabricated has attracted much interest recently. Carbon nanotube (CNT), with its advantages of fast carrier relaxation time, high damage threshold, and easy integration with fiber, has emerged the earliest carbon material proposed as saturable absorber for passively mode-locked lasers since 10 years ago. Although the size and wall number dependent optical absorption makes the CNT a band-selective saturable absorber, Wang et al. collected the CNTs with different diameters and chiralities to form a nanotube−polycarbonate film for wideband passive mode-locking with tuning range up to 40 nm.[4] Kivistö et al. also used a CNT-based saturable absorber mirror with varied diameters from 1.2 to 1.8 nm to demonstrate the passively mode-locked fiber lasers with tunable wavelength from 1.05 to 1.99 μm.[5] Due to the Dirac cone-like electronic band-structure, graphene has shown many unique optical properties, including near-ballistic transport,[6] Pauli blocking effect under strong illumination, and broadband saturable absorption.[7] Several studies have demonstrated that graphene can be exploited as a broadband saturable absorber for passively mode-locked fiber lasers with central wavelengths varied from visible to infrared region.[8−12] Similar materials such as nanoscale graphite,[13] charcoal powder,[14] and few-layer graphene nanosheets[15] were successively reported as alternatives. Recently, it was proposed that the simplest 3D topological insulator (TI)[16] could also function as a new class of saturable absorber because of its unique single Dirac cone surface state structure.[17]

Until recently, the Bi_2Te_3 crystals were identified as the 3D TIs with their Dirac surface states analyzed by angle-resolved photoelectron spectroscopy (ARPES),[18] and the carrier mobility on the Bi_2Te_3 surface was measured as high as ~5000 $cm^2/(V\ s)$.[19] Because the Dirac-like linear dispersion band on the surface states of Bi_2Te_3 crystals with a narrow energy bandgap of ~0.17 eV[20] resembles that of graphene, it is expected to apply the broadband saturable absorption property for passive mode-locking with a large wavelength tunability. The first experiment with either Bi_2Se_3 nanoplatelets synthesized via the polyol method[21] and Bi_2Te_3 nanosheets synthesized via hydrothermal intercalation/exfoliation[22] for

Received: August 25, 2014
Published: March 4, 2015

DOI: 10.1021/acsphotonics.5b00031
ACS Photonics 2015, 2, 481−490

picosecond pulse generation from EDFL were demonstrated. Recently, the Bi_2Te_3 TI has experimentally exhibited its saturable absorption with tuning ranging from 0.8 to 1.93 μm.[23,24] In addition, the layer-number dependent nonlinear optical property of TI has also been demonstrated.[25] Nevertheless, the Bi_2Te_3 is a TI material with vacancy and antisite-based crystalline defects such that the intrinsic Bi_2Te_3 crystal is naturally n-type. The Sn dopants are needed to compensate the vacancies and antisites to obtain the p-type $(Bi_{1-x}Sn_x)_2Te_3$ crystal with its bulk and surface electronic properties changed accordingly by increasing the Sn doping concentration. In previous work, the p-type Bi_2Te_3 nanoparticle with lower Fermi level can reduce the mode-locking threshold, thus, providing the passively mode-locked EDFL with less pumping power.[26] The result indicates that the saturable absorbance of TI may be related to its dopant type; however, the dopant-type dependent nonlinear optical property of TI has yet to be investigated.

In this work, the passive mode-locking of EDFL by using mechanically triturated Bi_2Te_3 nanoparticles with different dopant types as a new class of saturable absorber is preliminarily demonstrated. In contrast to the early report, this work tends to declare for the first time the density-of-state detuned Pauli blocking effect and to manipulate the saturable absorbance via different types of doping. In particular, both the complicated pulse shortening procedure and the competition between hybrid mode-locking mechanisms in the Bi_2Te_3 nanoparticle mode-locked EDFL system has been elucidated. Without chemical reactions, a simplified physical synthesis with a mortar based grinding process enables the size shrinkage of the Bi_2Te_3 nanoparticles to 200−300 nm. By directly imprinting these nanopowders onto the single-mode fiber (SMF) patchcord and controlling its coverage ratio, the linear transmittance in the passively mode-locked EDFL cavity is significantly improved for shortening the pulse width. The broadband saturable absorptions of these Bi_2Te_3 nanoparticles at 800 and 1570 nm are investigated. Soliton pulsation and shortening are started with the appropriate designation on self-phase modulation (SPM) and group-velocity dispersion (GDD) in the EDFL cavity, thus, providing sub-400 fs pulses both from the n- and p-type Bi_2Te_3 mode-locked EDFLs. The dopant-type dependent saturable absorption of Bi_2Te_3 TIs with respect to their passive mode-locking performances is compared. The great impact of the position of Fermi level on the saturated density of photoexcited carriers is analyzed to correlate well with the mode-locking threshold and the saturation intensity of the saturable absorber. Accordingly, such a novel method is proposed to enable the control on the self-amplitude modulation (SAM) of TI or by adjusting its dopant type.

RESULTS AND DISCUSSION

The irregular morphology of these nanoscale powders with an average size of 200−300 nm were characterized by scanning electron microscope (SEM), as shown in Figure 1a. Both the n- and p-type Bi_2Te_3 nanoparticles were directly grinded, first in a mortar and then in the triturator.[27] Afterward, these two types of Bi_2Te_3 nanoparticles were directly coated onto the end-faces of single-mode fiber (SMF) patchcords with their coverage ratios precisely controlled to maintain the linear transmittance at 75 and 85%, which were then connected with other SMF patchcords to insert these Bi_2Te_3 nanoparticles into the EDFL cavity. Figure 1b shows the 500× magnified optical microscopy

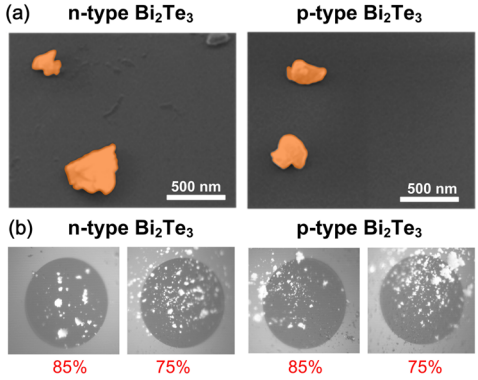

Figure 1. (a) SEM images and (b) OM images of n- and p-type Bi_2Te_3 nanoparticles coated on the SMF connector end-face with different linear transmittances.

(OM) images of Bi_2Te_3 nanoparticles on the end-face of the SMF patchcord.

To reveal the core composition and bonding properties of bismuth and tellurium atoms in the n- and p-type Bi_2Te_3 nanoparticles, the static X-ray photoelectron spectroscopy (XPS) was used for near-surface analysis within a depth of a few nanometers. The high-resolution XPS scans of the Bi 4f spectra are shown in Figure 2a,c, which indicate two main peaks at 162.5 and 157.1 eV correlated with the observed binding energies of Bi $4f_{5/2}$ and Bi $4f_{7/2}$ of Bi_2Te_3. In addition, the peaks located at 158.5 and 163.8 eV infer the coexistence of the Bi_2O_3-based surface states. The Te 3d spectra shown in Figure 2b,d reveal two peaks at 582.3 and 572.0 eV, which match well the reported binding energies of Te $3d_{3/2}$ and Te $3d_{5/2}$ of Bi_2Te_3. Similarly, the peaks located at 586.2 and 575.7 eV within the Te 3d spectra confirm the existence of TeO_2-based surface states.[28]

The relative peak intensities from the XPS spectra facilitate the calculation on the ratio of the peak value of Bi $4f_{7/2}$ to that of Te $3d_{5/2}$ (denoted as $R_{Bi/Te}$) for the Bi_2Te_3 with different types. The $R_{Bi/Te}$ ratios are 0.88 for n-type Bi_2Te_3 and 0.25 for p-type Bi_2Te_3, where the lower $R_{Bi/Te}$ ratio for p-type Bi_2Te_3 indicates that more Sn dopants replace the Bi atoms in the Bi_2Te_3 unit cell, which leads to a lower Fermi level of Bi_2Te_3. In addition, both doping types of Bi_2Te_3 nanoparticles consist of many oxidized defects on their surface, but they would not substantially influence the electronic property of Bi_2Te_3 surface states. Because the surface states of TIs are typically changed by spin−orbit coupling with their conduction and valence bands crossing over once, this time-reversal invariant band structure of topological material leads to an anomalous phenomenon of forbidden backscattering.[29,30] This unique characteristic makes the electron experience little or no resistance when propagating along the surface of the Bi_2Te_3 nanoparticles, which retains the saturated absorption property even with numerous oxidized defects on the TI material surface.

The Raman scattering spectrum of the Bi_2Te_3 nanoparticle is shown in Figure 3. Three Raman optical phonon peaks representing the A_{1g}^1, E_g^2, and A_{1g}^2 signals are located at 61, 88, and 134 cm^{-1}, respectively.[31] The peak positions are very close to the previously measured and assigned Raman peaks of bulk crystalline Bi_2Te_3. However, an additional peak with significant intensity appeared at ∼119 cm^{-1} in the Raman spectrum and was identified as an A_{1u} mode composed of longitudinal optical (LO) phonons at the BZ boundary (Z point). The A_{1u} mode is

DOI: 10.1021/acsphotonics.5b00031
ACS Photonics 2015, 2, 481−490

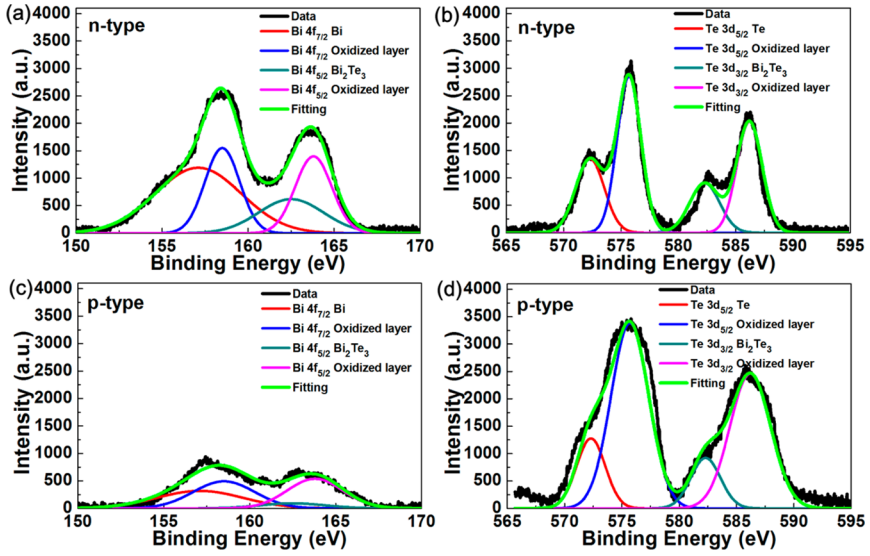

Figure 2. (a) Bi 4f and (b) Te 3d of the n-type Bi_2Te_3 nanoparticles, and (c) Bi 4f and (d) Te 3d XPS spectra of the p-type Bi_2Te_3 nanoparticles.

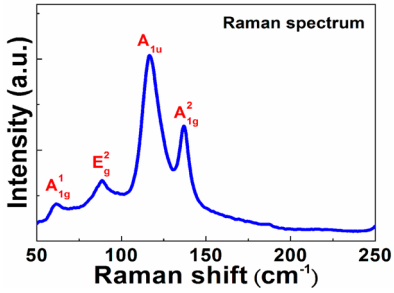

Figure 3. Raman spectra for the Bi_2Te_3 nanoparticles.

an IR active mode but not Raman active mode in bulk Bi_2Te_3 crystals. Thus, the Raman scattering spectra of the n- and p-type Bi_2Te_3 nanoparticles demonstrate that the active mode (A_{1u}) must be odd parity and is Raman forbidden for bulk crystal due to its inversion symmetry, which is activated to show the breaking up of the crystalline symmetry of Bi_2Te_3 nanoparticles when reducing their radius down to 200−300 nm.

Subsequently, the dynamic absorption of light by the surface states of the n- and p-type Bi_2Te_3 are demonstrated in Figure 4. The electrons are excited by the incident light from the valence

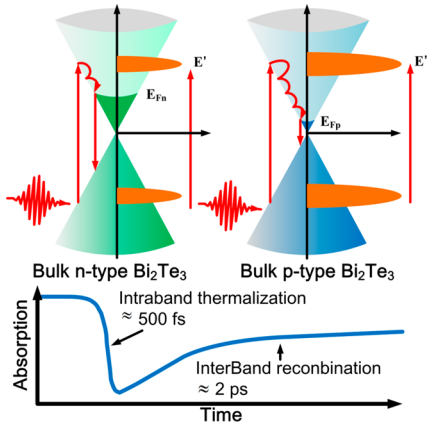

Figure 4. Dynamic absorption of light by the surface states of Bi_2Te_3.

band into the conduction band. Afterward, these hot electrons rapidly thermalize, cool down and eventually form a hot Fermi−Dirac distribution. It was found that the intraband thermalization and cooling process of photoexcited carriers on the surface of Bi_2Te_3 takes approximately 500 fs.[32] Under high-intensity incidence, the nonlinear absorption of the TI based saturable absorber is correlated with the Pauli's blocking effect which occurs when the states of conduction band at energies between E_c and $E_{photon} - E_g$ are fulfilled with photoexcited carriers. With the reduction or vanishing of optical illumination, intraband phonon scattering continues to cool the thermalized carriers. The interband recombination finally resumes the excited carriers and recovers the optical absorption back to their thermal equilibrium condition within 2 ps.[32] The absorption of photons inside the saturable absorber at a transition energy ceases owing to the band filling, and the photocarrier density n is simply related to the input light intensity I, carrier recombination time τ and light frequency ν, as given by $n = \alpha I\tau/h\nu$.[8,33] Therefore, the nonlinear absorbance can be related to the density of photoexcited carriers (n_{in}) and the saturated density of photoexcited carriers (n_{sat}) in the TI. The saturable transmittance versus the pulsed peak power is expressed as

$$T = \exp(-\alpha) = \exp\left[-\left(\alpha_{lin} + \frac{\alpha_{non}}{1 + I_{in}/I_{sat}}\right)\right] = \exp\left[-\left(\alpha_{lin} + \frac{\alpha_{non}}{1 + n_{in}/n_{sat}}\right)\right] \quad (1)$$

where I_{in} and I_{sat} are the input and saturation intensities, respectively; α is the absprbance of saturable absorber consisting of α_{lin} and $\alpha_{non}/(1 + I_{in}/I_{sat})^{-1}$. The α_{lin} can be obtained in saturated (extremely large intensity) condition, whereas $\alpha_{lin} + \alpha_{non}$ is obtained when input intensity is extremely small. The absorbance is defined as $\alpha = -\ln(T)$. The normalized absorbance is calculated to compare the modulation depth among different samples in convenience. In the particular case of the TI, the saturation intensity can be also modified if the allowable density of states for photoexcited carriers is detuned by the doping type and the concentration. Because the

DOI: 10.1021/acsphotonics.5b00031
ACS Photonics 2015, 2, 481−490

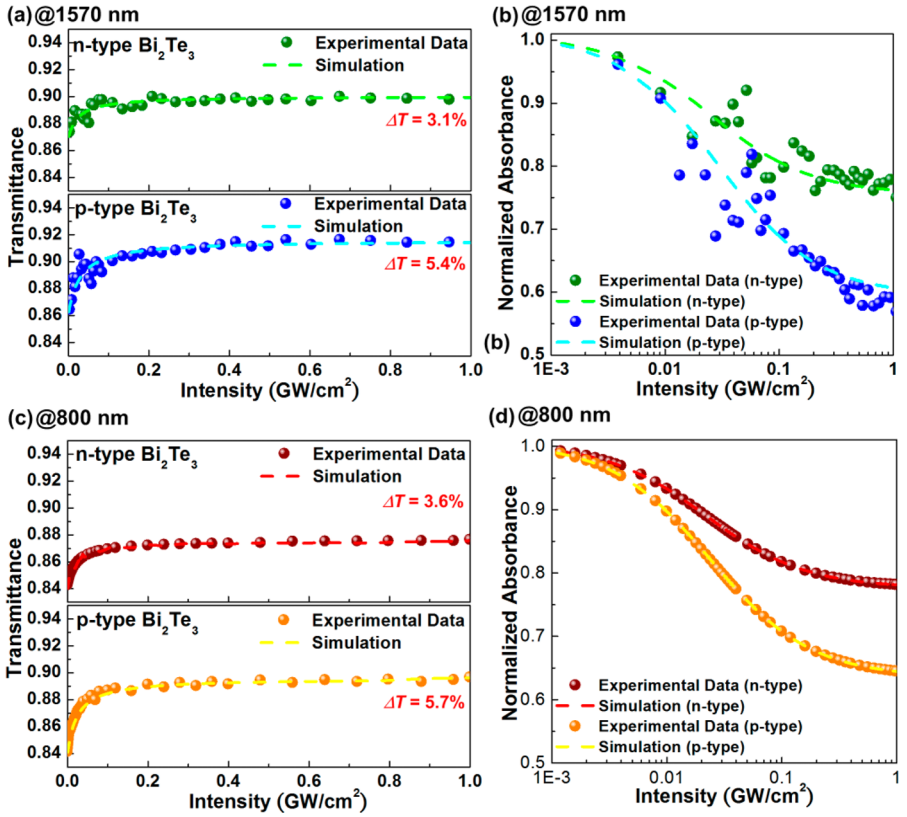

Figure 5. (a) Nonlinear transmittance and (b) normalized absorbance of n- and p-type Bi_2Te_3 nanoparticles at 1570 nm. (c) Nonlinear transmittance and (d) normalized absorbance of n- and p-type Bi_2Te_3 nanoparticles at 800 nm.

Fermi energy of the n-type Bi_2Te_3 is higher than those of the intrinsic Bi_2Te_3 and p-type Bi_2Te_3, the saturated density of photoexcited carriers in the p-type Bi_2Te_3 (n_p) is larger than those in the intrinsic Bi_2Te_3 (n_i) and the n-type Bi_2Te_3, as written by

$$n_{n,sat} = \int_{E_{Fn}}^{E_{photon}-E_{Fn}} D(E)f(E)dE < n_{i,sat} < \int_{E_{Fp}}^{E_{photon}-E_{Fp}} D(E)f(E)dE = n_{p,sat} \quad (2)$$

where $D(E)$ denotes the density of states (DOS) at the energy E, $f(E)$ the probability distribution function of carriers, E_{photon} the energy of photon-excited electrons, E_{Fn} and E_{Fp} are the Fermi energies of n- and p-type Bi_2Te_3, respectively. That is, the p-type Bi_2Te_3 possesses the highest α_{non} and I_{sat}, as compared to those of the intrinsic Bi_2Te_3. In contrast, the n-type Bi_2Te_3 exhibits the smallest α_{non} and I_{sat} among three types of TIs.

The Bi_2Te_3 TI with a narrow energy bandgap of ~0.17 eV is expected to apply the broadband saturable absorption property for passive mode-locking.[20] Chen et al. have experimentally demonstrated the saturable absorption of intrinsic Bi_2Te_3 at 800 and 1550 nm by z-scan analyses.[23] In principal, the dopant-type of TI only shifts the Fermi level without changing its energy bandgap. That is, the photocarrier density and saturated photocarrier density are different in n- and p-type Bi_2Te_3; however, the property of broadband saturable absorption is still existed in both n- and p-type Bi_2Te_3. To confirm the point of view on the broadband saturable absorption of n- and p-type Bi_2Te_3 nanoparticles, the nonlinear saturable absorbance of the n- and p-type Bi_2Te_3 nanoparticles were measured by varying the incident pulsed laser intensity at 1570 nm, as shown in Figure 5a,b. The excitation source was a pulsed fiber laser with central wavelength of 1570 nm and a pulse width of 300 fs. The improved transmittance is observed with increasing the pulse intensity, which is a key parameter for passive mode-locking of the EDFL. The saturable transmittance for both types of Bi_2Te_3 are numerically simulated by eq 1 with α_{non} of 0.033 and 0.065, α_{lin} of 0.105 and 0.088, and I_{sat} of 25 and 29 MW/cm^2 for n- and p-type Bi_2Te_3, respectively. As a supporting evidence, their nonlinear saturable absorbance at different wavelengths (far from 1550 nm) are demonstrated in Figure 5c,d by using a passively mode-locked Ti:sapphire laser as the pumping source with central wavelength, pulse width, and repetition rate of 800 nm, 100 fs, and 80 MHz, respectively. For n-type Bi_2Te_3 nanoparticle, the transmittance is increased from 0.84 to 0.876 with ΔT of 0.036; For p-type Bi_2Te_3 nanoparticle, the transmittance is increased from 0.84 to 0.897 with ΔT of 0.057. The nonlinear transmittance can be simulated by using eq 1. For n-type Bi_2Te_3 nanoparticle, the parameters of α_{lin}, α_{non}, and I_{sat} are 0.133, 0.039, and 21 MW/cm^2; For p-type Bi_2Te_3 nanoparticle, the parameters of α_{lin}, α_{non}, and I_{sat} are 0.11, 0.061, and 24 MW/cm^2. These experimental results prove that n- and p-type Bi_2Te_3 TIs can be served as the broadband saturable absorbers.

When the dominated pulse shortening mechanism in the EDFL is transferred from self-amplitude modulation (SAM) to SPM, the analytic hyperbolic secant pulse solution of a passively mode-locked soliton laser model under the interactions between GDD and SPM can be derived from the Haus master equation, and the minimal full-width at half-maximum (fwhm) pulse width τ_{fwhm} is dominated by the nonlinear absorbance, as given by[34]

DOI: 10.1021/acsphotonics.5b00031
ACS Photonics 2015, 2, 481−490

$$\tau_{\mathrm{fwhm}} = \frac{1.76}{2}\sqrt{\frac{2D_g}{\alpha_{\mathrm{non}}}} \quad (3)$$

where D_g is the gain dispersion. According to the numerically simulated values obtained from the saturation transmittance, the passively mode-locked EDFL with a p-type Bi_2Te_3 based saturable absorber can generate shorter pulse width than that with the n-type Bi_2Te_3.

Figure 6 shows the configuration of the passively mode-locked EDFL ring cavity with a bidirectional pumping scheme.

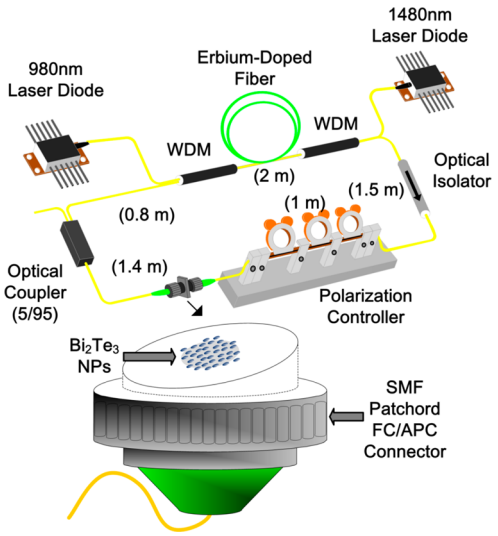

Figure 6. Configuration of Bi_2Te_3 nanoparticle saturable absorber based passively mode-locked EDFL system.

A 2 m long high-gain Erbium-doped fiber (LIEKKITM Er80−8/125) was bidirectionally pumped by two laser diodes (LDs) at central wavelengths of 980 nm (forward) and 1480 nm (backward) via two wavelength-matched wavelength division multiplexing couplers (WDMs). When operating both LDs at 900 mA, the LDs deliver pumping powers as much as 290 mW at 980 nm and 200 mW at 1480 nm. An optical isolator was utilized to fix the unidirectional propagation of the circulated pulse and eliminate the intracavity reflection to stabilize the passive mode-locking. A polarization controller (PC) inserted before the Bi_2Te_3 nanoparticles based saturable absorber was properly adjusted to optimize the intracavity polarization of the EDFL. The 1 × 2 optical coupler provides 5% for output and 95% for feedback into the cavity. The length of SMF with a dispersion coefficient of $\beta_{2,\mathrm{SMF}} = -20$ ps^2/km is 4.7 m, and the length of EDF with $\beta_{2,\mathrm{EDF}} = -20$ ps^2/km is 2 m. As a result, the cavity GDD is −0.134 ps^2.

After inserting the Bi_2Te_3 nanoparticle-based saturable absorber into the EDFL cavity, a stably mode-locked EDFL pulse train can be obtained without altering the polarization controller or vibrating the intracavity fiber segment, which confirms that the Bi_2Te_3 saturable absorber has taken the place to dominate the passive mode-locking in the EDFL. Figure 7 depicts the autocorrelation trace and optical spectra of the passively mode-locked EDFL varied with the n-type Bi_2Te_3 nanoparticle-based saturable absorbers. The autocorrelation traces and optical spectra were measured using an autocorrelator (Femtochrome FR-103XL) and an optical spectrum analyzer (Ando AQ6317B), respectively. For the EDFL passively mode-locked with n-type Bi_2Te_3, the pulse width can be shortened from 499 to 400 fs and the spectral fwhm can be broadened from 5.35 to 6.56 nm by enlarging the linear transmittance of the saturable absorber from 75 to 85%. The time-bandwidth products (TBPs) of both experimental results are approximately 0.32.

In contrast, the pulse width of the EDFL passively mode-locked by p-type Bi_2Te_3 is relatively short, which slightly

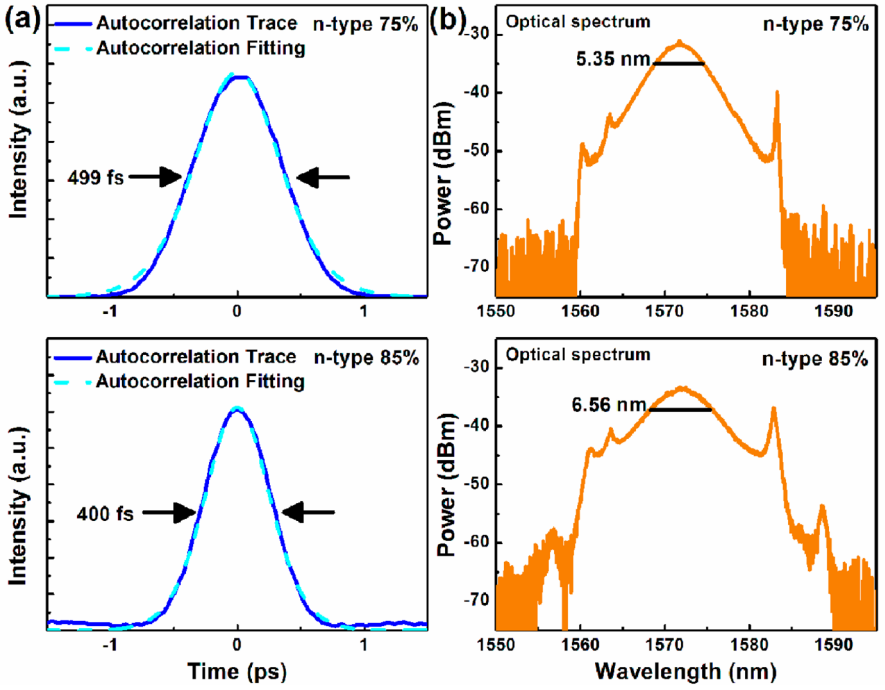

Figure 7. (a) Autocorrelation traces and (b) optical spectra of the passively mode-locked EDFLs by the n-type Bi_2Te_3 nanoparticle based saturable absorber under different linear transmittances.

DOI: 10.1021/acsphotonics.5b00031
ACS Photonics 2015, 2, 481−490

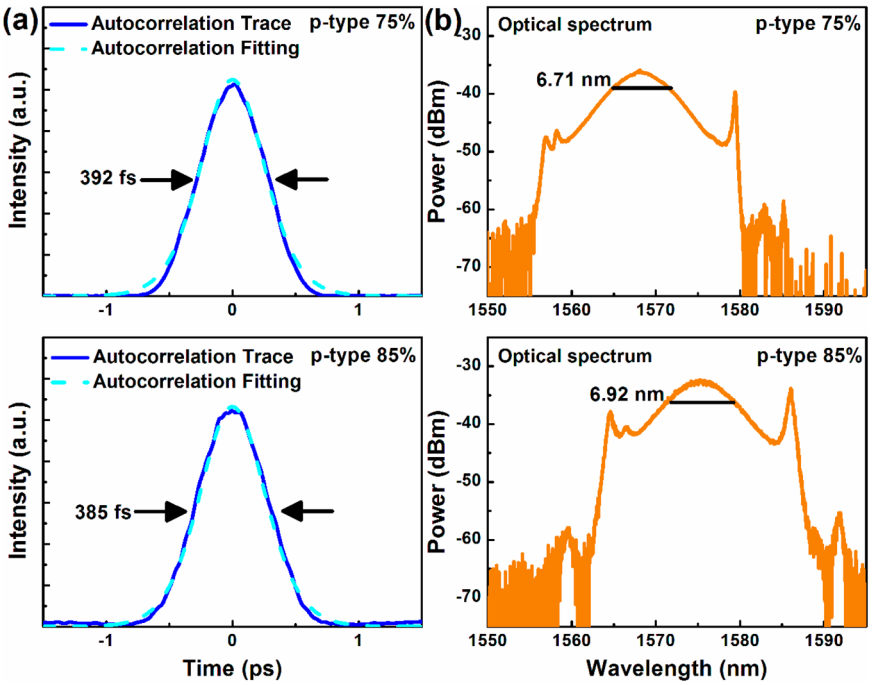

Figure 8. (a) Autocorrelation traces and (b) optical spectra of the passively mode-locked EDFLs by the p-type Bi_2Te_3 nanoparticle-based saturable absorber under different linear transmittances.

reduces from 392 to 385 fs with corresponding spectral fwhm broadened from 6.71 to 6.92 nm by increasing the linear transmittance of the saturable absorber from 75 to 85%, as shown in Figure 8. The TBPs of both experimental results are approximately 0.32. As expected, the p-type Bi_2Te_3 saturable absorber generates much shorter pulse width than the n-type Bi_2Te_3 saturable absorber, as contributed by the larger saturable absorbance and modulation depth of the p-type Bi_2Te_3. In this work, the highly chirped dissipative soliton inevitably results in a TBP away from the transform-limited regime (TBP = 0.315), which originates from the interaction of linear GDD and the nonlinear SPM at a specific designation on net gain and cavity length.[35] In particular, the enhanced resonance of first- and second-order Kelly sidebands indicated by the arrow in Figure 9b, with frequency offsets of ν_1 = 1.31 THz and ν_2 = 1.94 THz

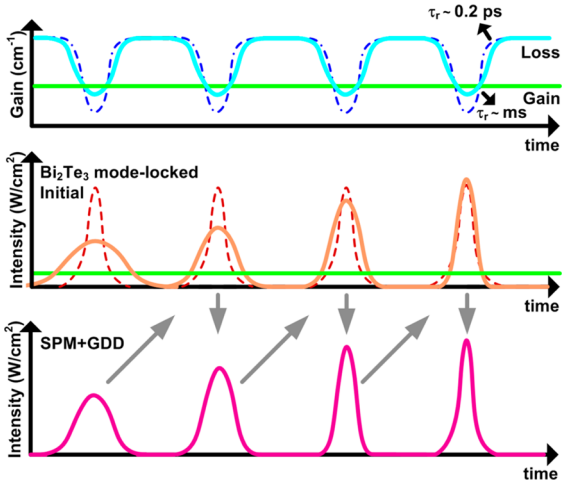

Figure 9. Schematic of the SPM-GDD combined compression for the Bi_2Te_3-based mode-locked fiber laser.

can be observed only with linear transmittance of 85%, indicating that the pulses may experience highly saturated gain in the EDF.[36]

Due to the small saturation intensity of both n- and p-type Bi_2Te_3 nanoparticles, these materials cannot create sufficient extinction between the gain and the saturable loss in the EDFL cavity, which inevitably results in a broader pulse when employing saturable absorbers with lower saturation intensity. To overcome this drawback, efficient pulse compression either via a strong SPM or an additional mode-locking mechanism coexisting in the cavity is preferred.[37] However, SPM is an intensity dependent effect that strictly relies on not only raising the peak power, but also on reducing the pulse width of the circulated pulses. Figure 9 demonstrates the schematic of the SPM-GDD combined compression for the Bi_2Te_3-based mode-locked fiber laser. Due to the fact that the finalized pulse width can enter the soliton regime, it is understood that the initial EDFL pulse width mode-locked by the Bi_2Te_3 saturable absorber is in an incomplete mode-locking state, and the subsequent SPM effect gradually enhanced at a specifically designed cavity with appropriately adjusted GDD at a slight value plays a more important role on the intracavity pulse compression.

In addition, even a weak birefringence effect naturally occurred in the EDFL cavity can induce a residual polarization-dependent loss inside the cavity, which would also initiate another less dominant passive mode-locking mechanism (i.e., the nonlinear polarization rotation) by introducing an artificial saturable loss condition to assist the Bi_2Te_3-based saturable absorber. Although Zhao et al. wondered that the nonlinear polarization rotation (NPR) effect is hardly induced without a polarizer in the cavity,[38] the weak nonlinear polarization phenomenon can be still existed in the EDFL cavity even constructed with polarization insensitive components.[39,40] Even without a polarizer inside the EDFL cavity, the combination of residual birefrigence in those passive

DOI: 10.1021/acsphotonics.5b00031
ACS Photonics 2015, 2, 481−490

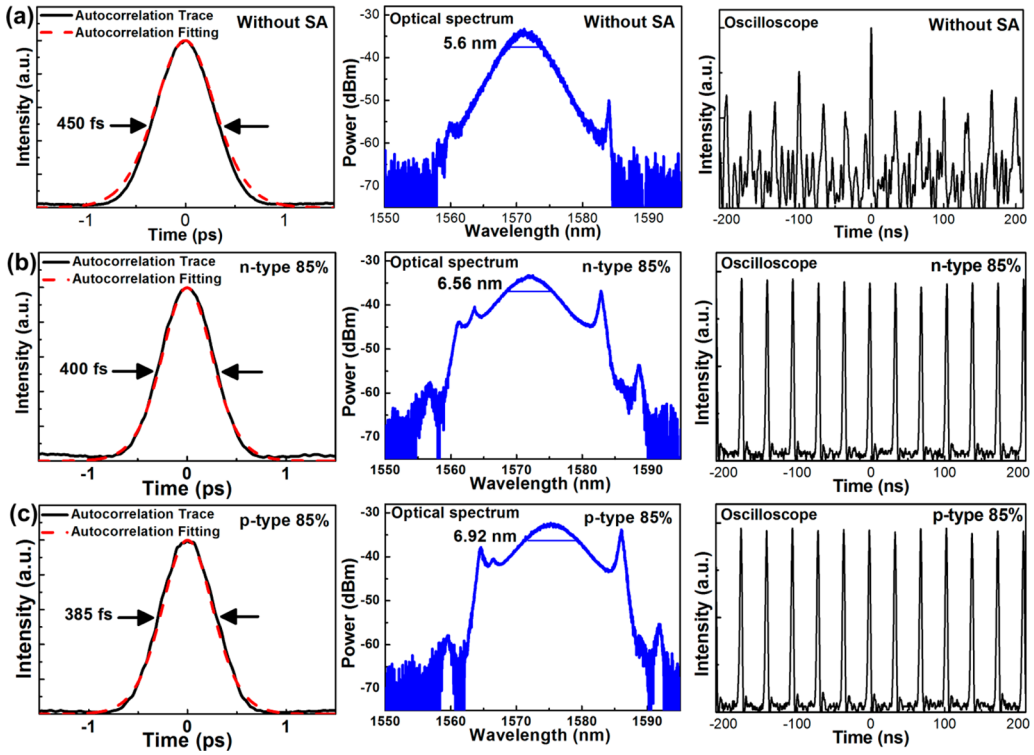

Figure 10. Autocorrelation traces, optical spectra, and oscilloscope traces of the passively mode-locked EDFLs. (a) Without the Bi_2Te_3 nanoparticle, and (b) with the n-type and (c) p-type Bi_2Te_3 nanoparticles.

components (SMF, EDF, and optical isolator etc.) could induce the residual NPR effect to form an artificial saturable absorber.[41] This is one of the possible reasons why Jeong et al. can change the carbon nanotube passively mode-locked EDFL pulse width from 1.6 ps to 470 fs by adjusting the variation of polarization state.[42] However, the mode-locked EDFL pulse width may not be shortened and cannot vary too much if the residual NPR effect is really weak. With such effect, the current EDFL may initiate a weak but unstable pulse via a strictly difficult adjustment on the phase of intracavity polarization. Figure 10 demonstrates the autocorrelation trace and optical spectrum of such a weakly mode-locked EDFL pulse. The pulse width and spectral full-width at half-maximum (fwhm) are 450 fs and 5.75 nm, with the corresponding time-bandwidth product (TBP) of 0.32. The oscilloscope trace shows an unstable output from the EDFL cavity with a carrier amplitude jitter (CAJ) as high as 13.9%,[43] which is hardly survived for 10 min. The instability of such weak mode-locking mechanism caused by the NPR induced from residual birefringence of passive components makes the system inapplicable to researches.

After inserting Bi_2Te_3 nanoparticle saturable absorber into the EDFL cavity, a stabilized passive mode-locking of the EDFL with shortened pulse width can be obtained. Figure 10b,c provides the autocorrelation traces, optical spectra, and oscilloscope traces of the EDFLs passively mode-locked with n- and p-type Bi_2Te_3 nanoparticles, respectively. The pulse widths of the EDFL passively mode-locked by the n- and p-type Bi_2Te_3 nanoparticles are 400 and 385 fs with corresponding spectral fwhm of 6.56 and 6.92 nm, respectively. The oscilloscope traces confirm that the pulse trains are stably initiated by n- and p-type Bi_2Te_3 nanoparticles with lower CAJ values of 1.71 and 1.73%, respectively. According to the experimental results, more than one mode-locking mechanism existed in the EDFL cavity can contribute the self-amplitude modulation; however, the generated EDFL pulses are dominated by Bi_2Te_3 nanoparticle-based saturable absorption effect. An ideal saturable absorber for passively mode-locked lasers is expected to possess the characteristics of broadband absorption, ultrafast carrier relaxation time, low saturable intensity, large modulation depth, and high damage threshold. Graphene and TIs have shown great potential to be the nice saturable absorbers. Hereafter, the parametric comparisons between graphene and Bi_2Te_3 (obtained by our group and others) have been addressed. The related parameters of graphene and TI saturable absorbers are shown in Table 1.

Table 1. Related Parameters of Graphene and TI Saturable Absorbers

	graphene	Bi_2Te_3
saturable absorption range	0.8[11]−2.9 μm (passive Q-switching)[44]	0.8[22]−1.93 μm[24]
carrier relaxation time (intraband/interband)	~0.1/~1.6 ps[8,45]	~0.5/~2 ps[32]
saturation intensity	0.71 MW/cm^2[28]	Bi_2Te_3: 31 MW/cm^2[49]
self-amplitude modulation (SAM) coefficient	0.068 cm^2/MW[46]	0.002 cm^2/MW (our work)
optical damage threshold	2.7 TW/cm^2 at 790 nm[47]	28 GW/cm^2 at 800 nm[23]

Based on these requested features, graphene was preliminarily demonstrated as a saturable absorber for passively mode-locked fiber lasers, which exhibits broadband absorption from 0.8 to 2.9 μm[11,44] due to its zero bandgap property. The ultrafast relaxation in graphene was also reported with intraband carrier−carrier relaxation time of ~0.1 ps[45] and interband relaxation time of ~1.6 ps.[8] The self-amplitude

DOI: 10.1021/acsphotonics.5b00031
ACS Photonics 2015, 2, 481−490

modulation (SAM) coefficient ($\gamma \propto \alpha_{non}/I_{sat}$) of graphene-based saturable absorber can potentially be large due to its extremely small I_{sat} of 0.71 MW/cm;[28] however, the transmittance of a single-layer graphene in visible and infrared regions is as high as 0.97 to reduce the nonlinear absorbance as well as the SAM coefficient.[8] Moreover, graphene can also sustain high optical intensity of >2.7 TW/cm^2 (@790 nm) to prevent the thermal problem and maintain the stability of laser.[47] As an alternative candidate, the TI also possesses a Dirac-like band structure with a small bandgap to serve as a broadband saturable absorber at wavelength ranging between violet and mid-infrared.[48] According to previous reports, the saturable absorption behavior of Bi_2Te_3 has been demonstrated at wavelengths extended from 0.8 to 1.93 μm.[23,24] The intraband and interband carrier relaxation times of Bi_2Te_3 were measured as ~0.5 and ~2 ps,[32] which are comparable to that of graphene. Bi_2Te_3 saturable absorber reveals a high saturation intensity of ~31 MW/cm^2 and high nonlinear absorbance to cause a comparable SAM coefficient.[49] This makes Bi_2Te_3 better than graphene when serving as the saturable absorber in fiber lasers with high output power. Zhao et al. have performed that Bi_2Te_3 could exhibit a very low transmittance of <0.04 and a large increased transmittance ΔT of 0.953.[22] Bi_2Te_3 saturable absorber can sustain the optical intensity of ~28 GW/cm^2 (@800 nm) without the thermal damage.[23]

CONCLUSION

In conclusion, the effect of doping types of nanoscale Bi_2Te_3 saturable absorbers on the passive mode-locking performance of the EDFL is investigated. A novel method for enabling the control on the SAM of TI by adjusting its dopant type is developed. In addition, both the complicated pulse shortening procedure and the competition between hybrid mode-locking mechanisms in the Bi_2Te_3 nanoparticle mode-locked EDFL system has been elucidated. The directly brushed Bi_2Te_3 powder shrinks the SMF connecter spacing to reduce the coupling loss. The dopant-type of TI only shifts the Fermi level without changing its energy bandgap, that the n- and p-type Bi_2Te_3 nanoparticles have shown the broadband saturable absorption at 800 and 1570 nm. The time-reversal-invariant band diagram of the Bi_2Te_3 nanoparticle surface maintains the saturable absorption property at 1570 nm, providing the nonsaturated losses of 0.033 and 0.065, linear losses of 0.105 and 0.088, and saturation intensities of 25 and 29 MW/cm^2 for n- and p-type Bi_2Te_3, respectively. The time-reversal-invariant band of surface states preserves the saturable absorption property, and hence, more vacancies for excited carriers are provided by surface states of the p-type Bi_2Te_3 with a lower Fermi level, which causes larger nonsaturated loss and saturation intensity to provide a much shorter pulse width (385 fs) at the SAM case. In comparison, the EDFL with a n-type Bi_2Te_3 saturable absorber relies on strong SPM and negative GDD effects to further compress its soliton pulse width from 499 to 400 fs, comparable with that of a p-type Bi_2Te_3, while both first- and second-order Kelly sidebands are observed with frequency offsets of 1.31 and 1.94 THz.

METHODS

Fabrications of n- and p-Type Bi_2Te_3 Nanoparticles. Both the n- and p-type Bi_2Te_3 nanoparticles were directly grinded, first in a mortar and then in a triturator, as shown in Figure 11a. After the mechanical triturating process, both the n- and p-type Bi_2Te_3 nanoparticles with weight of 0.5 g were

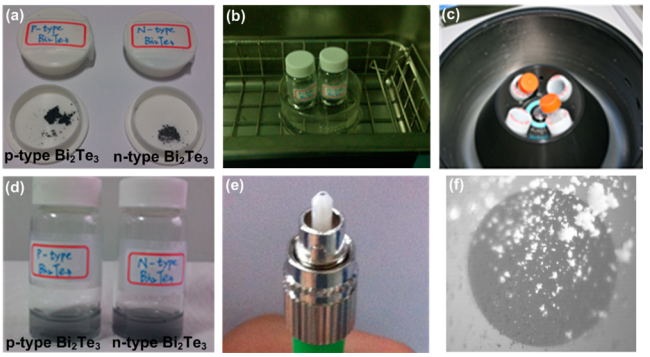

Figure 11. Fabrication process of n- and p-type Bi_2Te_3 nanoparticles. (a) Photograph of the triturated n- and p-type Bi_2Te_3 nanoparticles. (b) Process of ultrasonication for further separating the n- and p-type Bi_2Te_3 nanoparticles. (c) Photograph of the centrifugation. (d) After the centrifugation, the few-layer and small size Bi_2Te_3 nanoparticles were floated on the solution surface. (e) Adhesion of n- and p-type nanoparticles on the end-faces of SMF patchcords. (f) Photograph of Bi_2Te_3 nanoparticles on the end-face of SMF patchcord.

dispersed in acetone solution with a volume of 5 mL, respectively. The Bi_2Te_3 nanoparticles in the solution were further separated into small pieces by employing the ultrasonication process at 25 °C for 10 min, as demonstrated in Figure 11b. To extract the small-size Bi_2Te_3 nanoparticles, the Bi_2Te_3 nanoparticle solution was put in the centrifuge at 1000 rpm for 3 min (Figure 11c) to keep the few-layer and small size Bi_2Te_3 nanoparticles floating in the upper part of the solution (Figure 11d). Eventually, the acetone solution containing few-layer and small-size Bi_2Te_3 nanoparticles were dip onto the end-faces of different single-mode fiber (SMF) patchcord. After evaporating the chemical solvent in an oven at 80 °C for 5 min, the Bi_2Te_3 nanoparticles were self-adhered to the end-faces of the SMF patchcords, as illustrated in Figure 11e. By controlling the concentration of Bi_2Te_3 nanoparticle solution, the coverage ratio of Bi_2Te_3 nanoparticles on the patchcord end-face can be adjusted.

Characterizing the Linear Transmittance of n- and p-Type Bi_2Te_3 Nanoparticles. After adhering the Bi_2Te_3 nanoparticles onto the end-face of one SMF patchcord, another SMF patchcord was connected to sandwich the Bi_2Te_3 nanoparticles in between. To measure the linear transmittances of the n- and p-type Bi_2Te_3 nanoparticles, a continuous-wave (CW) tunable laser with an average power of 0 dBm at central wavelength of 1570 nm was utilized. After passing through the sandwiched patchcord/Bi_2Te_3/patchcord segment, the transmitted laser power was detected by a dual-port power meter and subtracted each other for noise suppression. With such a setup as shown in Figure 12, the linear transmittances of Bi_2Te_3 nanoparticle on the SMF patchcord end-face can be measured.

Characterizing the Saturable Absorbances of n- and p-Type Bi_2Te_3 Nanoparticles. An intensity-scan measurement was established to analyze the nonlinear absorbances of the n- and p-type Bi_2Te_3 nanoparticles; This measurement employs a mode-locked fiber laser with central wavelength of 1560 nm and a pulse width of 700 fs as the pumping source. The peak power of the laser pulse was enlarged with a boost erbium-doped fiber amplifier, and the excitation source was divided by a 50/50 coupler to directly measure the throughput

DOI: 10.1021/acsphotonics.5b00031
ACS Photonics 2015, 2, 481−490

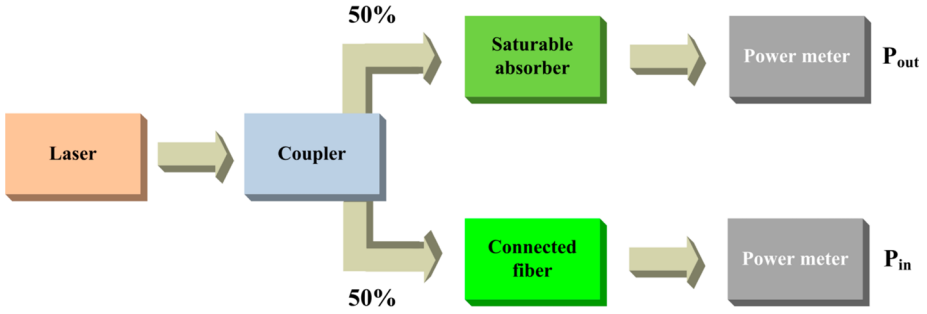

Figure 12. Experimental setup for analyzing the linear (unsaturated) and nonlinear (saturated) transmittance.

power with and without passing through the Bi_2Te_3 nanoparticles. The transmittance was obtained by calculating the ratio between two coupling lights without the influence of power and shape fluctuations.

AUTHOR INFORMATION

Corresponding Author

*Phone: +886-2-33663700, #235. Fax: +886-2-33669598. E-mail: grlin@ntu.edu.tw.

Notes

The authors declare no competing financial interest.

ACKNOWLEDGMENTS

This work was supported by the Ministry of Science and Technology, Taiwan, R.O.C., and the Excellent Research Projects of National Taiwan University, Taiwan, under Grants NSC 100-2221-E-002-156-MY3, NSC 101-2221-E-002-071-MY3, MOST 103-2221-E002-042-MY3, NTU103R89081, and NTU103R89083.

REFERENCES

(1) Gattass, R. P.; Mazur, E. Femtosecond laser micromachining in transparent materials. *Nat. Photonics* **2008**, *2*, 219−225.
(2) Millard, A. C.; Wiseman, P. W.; Fittinghoff, D. N.; Wilson, K. R.; Squier, J. A.; Müller, M. Third-harmonic generation microscopy by use of a compact, femtosecond fiber laser source. *Appl. Opt.* **1999**, *38*, 7393−7397.
(3) Lin, G.-R.; Pan, C.-L.; Lin, Y.-T. Self-steepening of prechirped amplified and compressed 29-fs fiber laser pulse in large-mode-area Erbium-doped fiber amplifier. *J. Lightwave Technol.* **2007**, *25*, 3597−3601.
(4) Wang, F.; Rozhin, A. G.; Scardaci, V.; Sun, Z.; Hennrich, F.; White, I. H.; Milne, W. I.; Ferrari, A. C. Wideband-tuneable, nanotube mode-locked, fibre laser. *Nat. Nanotechnol.* **2008**, *3*, 738−742.
(5) Kivistö, S.; Hakulinen, T.; Kaskela, A.; Aitchison, B.; Brown, D. P.; Nasibulin, A. G.; Kauppinen, E. I.; Härkönen, A.; Okhotnikov, O. G. Carbon nanotube films for ultrafast broadband technology. *Opt. Express* **2009**, *17*, 2358−2363.
(6) Geim, K.; Novoselov, K. S. The rise of graphene. *Nat. Mater.* **2007**, *6*, 183−191.
(7) Lim, G.-K.; Chen, Z.-L.; Clark, J.; Goh, R. G. S.; Ng, W.-H.; Tan, H.-W.; Friend, R. H.; Ho, P. K. H.; Chua, L.-L. Giant broadband nonlinear optical absorption response in dispersed graphene single sheets. *Nat. Photonics* **2011**, *5*, 554−560.
(8) Bao, Q.; Zhang, H.; Wang, Y.; Ni, Z.; Yan, Y.; Shen, Z. X.; Loh, K. P.; Tang, D. Y. Atomic-layer graphene as a saturable absorber for ultrafast pulsed lasers. *Adv. Funct. Mater.* **2009**, *19*, 3077−3083.
(9) Zhang, H.; Bao, Q.; Tang, D.; Zhao, L.; Loh, K. P. Large energy soliton erbium-doped fiber laser with a graphene-polymer composite mode locker. *Appl. Phys. Lett.* **2009**, *95*, 141103.
(10) Sun, Z.; Hasan, T.; Torrisi, F.; Popa, D.; Privitera, G.; Wang, F.; Bonaccorso, F.; Basko, D. M.; Ferrari, A. C. Graphene mode-locked ultrafast laser. *ACS Nano* **2010**, *4*, 803−810.
(11) Baek, I. H.; Lee, H. W.; Bae, S.; Hong, B. H.; Ahn, Y. H.; Yeom, D. I.; Rotermund, F. Efficient mode-locking of sub-70-fs Ti:Sapphire laser by graphene saturable absorber. *Appl. Phys. Express* **2012**, *5*, 032701.
(12) Zhang, M.; Kelleher, E. J. R.; Torrisi, F.; Sun, Z.; Hasan, T.; Popa, D.; Wang, F.; Ferrari, A. C.; Popov, S. C.; Taylor, J. R. Tm-doped fiber laser mode-locked by graphene-polymer composite. *Opt. Express* **2012**, *20*, 25077−25084.
(13) Lin, G.-R.; Lin, Y.-C. Directly exfoliated and imprinted graphite nano-particle saturable absorber for passive mode-locking erbium-doped fiber laser. *Laser Phys. Lett.* **2011**, *8*, 880−886.
(14) Lin, Y.-H.; Lo, J.-Y.; Tseng, W.-H.; Wu, C.-I.; Lin, G.-R. Self-amplitude and self-phase modulation of the charcoal mode-locked erbium-doped fiber lasers. *Opt. Express* **2013**, *21*, 25184−25196.
(15) Yang, C.-Y.; Wu, C.-L.; Lin, Y.-H.; Tsai, L.-H.; Chi, Y.-C.; Chang, J.-H.; Wu, C.-I.; Tsai, H.-K.; Tsai, D.-P.; Lin, G.-R. Fabricating graphite nano-sheet powder by slow electrochemical exfoliation of large-scale graphite foil as a mode-locker for fiber lasers. *Opt. Mater. Express* **2013**, *3*, 1893−1905.
(16) Fu, L.; Kane, C.; Mele, E. Topological insulators in three dimensions. *Phys. Rev. Lett.* **2007**, *98*, 106803.
(17) Moore, J. E.; Balents, L. Topological invariants of time-reversal-invariant band structures. *Phys. Rev. B* **2007**, *75*, 121306.
(18) Chen, Y. L.; Analytis, J. G.; Chu, J. H.; Liu, Z. K.; Mo, S. K.; Qi, X. L.; Zhang, H. J.; Lu, D. H.; Dai, X.; Fang, Z.; Zhang, S. C.; Fisher, I. R.; Hussain, Z.; Shen, Z. X. Experimental realization of a three-dimensional topological insulator, Bi_2Te_3. *Science* **2009**, *325*, 178−181.
(19) Wang, K.; Liu, Y.; Wang, W.; Meyer, N.; Bao, L. H.; He, L.; Lang, M. R.; Chen, Z. G.; Che, X. Y.; Post, K.; Zou, J.; Basov, D. N.; Wang, K. L.; Xiu, F. High-quality Bi_2Te_3 thin films grown on mica substrates for potential optoelectronic applications. *Appl. Phys. Lett.* **2013**, *103*, 031605.
(20) Thomas, G. A.; Rapkine, D. H.; Van Dover, R. B.; Mattheiss, L. F.; Sunder, W. A.; Schneemeyer, L. F.; Waszczak, J. V. Large electronic-density increase on cooling a layered metal: doped Bi_2Te_3. *Phys. Rev. B* **1992**, *46*, 1553−1556.
(21) Zhao, C.; Zou, Y.; Chen, Y.; Wang, Z.; Lu, S.; Zhang, H.; Wen, S.; Tang, D. Y. Wavelength-tunable picosecond soliton fiber laser with topological insulator: Bi_2Se_3 as a mode locker. *Opt. Express* **2012**, *20*, 27888−27895.
(22) Zhao, C.; Zhang, H.; Qi, X.; Chen, Y.; Wang, Z.; Wen, S.; Tang, D. Y. Ultra-short pulse generation by a topological insulator based saturable absorber. *Appl. Phys. Lett.* **2012**, *101*, 211106.
(23) Chen, S.; Zhao, C.; Li, Y.; Huang, H.; Lu, S.; Zhang, H.; Wen, S. Broadband optical and microwave nonlinear response in topological insulator. *Opt. Mater. Express* **2014**, *4*, 587−596.
(24) Jung, M.; Lee, J.; Koo, J.; Park, J.; Song, Y. W.; Lee, K.; Lee, S.; Lee, J. H. A femtosecond pulse fiber laser at 1935 nm using a bulk-structured Bi_2Te_3 topological insulator. *Opt. Express* **2014**, *22*, 7865−7874.

DOI: 10.1021/acsphotonics.5b00031
ACS Photonics 2015, 2, 481−490

(25) Zhang, H.; Lu, S. B.; Zheng, J.; Du, J.; Wen, S. C.; Tang, D. Y.; Loh, K. P. Molybdenum disulfide (MoS_2) as a broadband saturable absorber for ultra-fast photonics. *Opt. Express* **2014**, *22*, 7249−7260.
(26) Lin, Y. H.; Yang, C. Y.; Lin, S. F.; Tseng, W. H.; Bao, Q.; Wu, C. I.; Lin, G.-R. Soliton compression of the erbium-doped fiber laser weakly started mode-locking by nanoscale p-type Bi_2Te_3 topological insulator particles. *Laser Phys. Lett.* **2014**, *11*, 055107.
(27) Lin, Y.-H.; Chi, Y.-C.; Lin, G.-R. Nanoscale charcoal powder induced saturable absorption and mode-locking of a low-gain erbium-doped fiber-ring laser. *Laser Phys. Lett.* **2013**, *10*, 055105.
(28) Fu, J.; Song, S.; Zhang, X.; Cao, F.; Zhou, L.; Li, X.; Zhang, H. Bi_2Te_3 nanoplates and nanoflowers: Synthesized by hydrothermal process and their enhanced thermoelectric properties. *CrystEngComm* **2012**, *14*, 2159−2165.
(29) Roushan, P.; Seo, J.; Parker, C. V.; Hor, Y. S.; Hsieh, D.; Qian, D.; Richardella, A.; Hasan, M. Z.; Cava, R. J.; Yazdani, A. Topological surface states protected from backscattering by chiral spin texture. *Nature* **2009**, *460*, 1106−1109.
(30) Seo, J.; Roushan, P.; Beidenkopf, H.; Hor, Y. S.; Cava, R. J.; Yazdani, A. Transmission of topological surface states through surface barriers. *Nature* **2010**, *466*, 343−346.
(31) Shahil, K. M. F.; Hossain, M. Z.; Goyal, V.; Balandin, A. A. Micro-Raman spectroscopy of mechanically exfoliated few-quintuple layers of Bi_2Te_3, Bi_2Se_3, and Sb_2Te_3 materials. *J. Appl. Phys.* **2012**, *111*, 054305.
(32) Hajlaoui, M.; Papalazarou, E.; Mauchain, J.; Lantz, G.; Moisan, N.; Boschetto, D.; Jiang, Z.; Miotkowski, I.; Chen, Y. P.; Taleb-Ibrahimi, A.; Perfetti, L.; Marsi, M. Ultrafast surface carrier dynamics in the topological insulator Bi_2Te_3. *Nano Lett.* **2012**, *12*, 3532−3536.
(33) Yu, H.; Zhang, H.; Wang, Y.; Zhao, C.; Wang, B.; Wen, S.; Zhang, H.; Wang, J. Topological insulator as an optical modulator for pulsed solid-state lasers. *Laser Photonics Rev.* **2013**, *7*, L77−L83.
(34) Ḱartner, F. X.; der Au, J. A.; Keller, U. Mode-locking with slow and fast saturable absorbers: what's the difference? *IEEE J. Sel. Top. Quant. Electron.* **1998**, *4*, 159−168.
(35) Haus, H. A.; Fujimoto, J. G.; Ippen, E. P. Structures for additive pulse mode locking. *J. Opt. Soc. Am. B* **1991**, *8*, 2068−2076.
(36) Dennis, M. L.; Duling, I. N., III Experimental study of sideband generation in femtosecond fiber lasers. *IEEE J. Quantum Electron.* **1994**, *30*, 1469−1477.
(37) Ḱartner, F. X.; Jung, I. D.; Keller, U. Soliton mode-locking with saturable absorbers. *IEEE J. Sel. Top. Quant. Electron.* **1996**, *2*, 540−556.
(38) Zhao, C.; Lu, S.; Qi, X.; Zhang, H.; Wen, S.; Tang, D. Response to Comment on 'Ultra-short pulse generation by a topological insulator based saturable absorber' [*Appl. Phys. Lett.* **2013**, *103*, 106101]. *Appl. Phys. Lett.* **2013**, *103*, 106102.
(39) Matsas, V. J.; Newson, T. P.; Richardson, D. J.; Payne, D. N. Self starting passively mode-locked fibre ring soliton laser exploiting nonlinear polarization rotation. *Electron. Lett.* **1992**, *28*, 1391−1393.
(40) Safioui, J.; Bernard, F.; Swaelens, M.; Massar, S.; Kockaert, P.; Emplit, P.; Gorza, S. P. Comment on "Ultra-short pulse generation by a topological insulator based saturable absorber" [*Appl. Phys. Lett.* **2012**, *101*, 211106]. *Appl. Phys. Lett.* **2013**, *103*, 106101.
(41) Ismail, M. A.; Tan, S. J.; Shahabuddin, N. S.; Harun, S. W.; Arof, H.; Ahmad, H. Performance comparison of mode-locked erbium-doped fiber laser with nonlinear polarization rotation and saturable absorber approaches. *Chin. Phys. Lett.* **2012**, *29*, 054216.
(42) Jeong, H.; Choi, S. Y.; Rotermund, F.; Yeom, D.-I. Pulse width shaping of passively mode-locked soliton fiber laser via polarization control in carbon nanotube saturable absorber. *Opt. Express* **2013**, *21*, 27011−27016.
(43) Lin, Y. H. Yang; Liou, C.-Y.; Yu, J.-H.; Lin, C.-P. G.-R. Using graphene nano-particle embedded in photonic crystal fiber for evanescent wave mode-locking of fiber laser. *Opt. Express* **2013**, *21*, 16763−16776.
(44) Zhu, G.; Zhu, X.; Balakrishnan, K.; Norwood, R. A.; Peyghambarian, N. Fe^{2+}:ZnSe and graphene Q-switched singly Ho^{3+}-doped ZBLAN fiber lasers at 3 μm. *Opt. Mater. Express* **2013**, *3*, 1365−1377.
(45) Bonaccorso, F.; Sun, Z.; Hasan, T.; Ferrari, A. C. Graphene photonics and optoelectronics. *Nat. Photonics* **2012**, *4*, 611−622.
(46) Lin, Y. H.; Yang, C.-Y.; Lin S.-F. Lin, G.-R. Triturating versatile carbon materials as saturable absorptive nano powders for ultrafast pulsating of erbium-doped fiber lasers. *Opt. Mater. Express* **2015**, *5*, 236−253.
(47) Roberts, A.; Cormode, D.; Reynolds, C.; Newhouse-Illige, T.; LeRoy, B. J.; Sandhu, A. S. Response of graphene to femtosecond high-intensity laser irradiation. *Appl. Phys. Lett.* **2011**, *99*, 051912.
(48) Zhang, H.; Liu, C.-X.; Qi, X.-L.; Dai, X.; Fang, Z.; Zhang, S. C. Topological insulators in Bi_2Se_3, Bi_2Te_3 and Sb_2Te_3 with a single Dirac cone on the surface. *Nat. Phys.* **2009**, *5*, 438−442.
(49) Sotor, J.; Sobon, G.; Abramski, K. M. Sub-130 fs mode-locked Er-doped fiber laser based on topological insulator. *Opt. Express* **2014**, *22*, 13244−13249.

DOI: 10.1021/acsphotonics.5b00031
ACS Photonics 2015, 2, 481−490